https://doi.org/10.5194/bg-2019-353
Preprint. Discussion started: 6 September 2019

Biogeosciences Discussions

Influence of oceanic conditions in the energy transfer efficiency estimation of a micronekton model

Audrey Delpech[1,2], Anna Conchon[2,3], Olivier Titaud[2], and Patrick Lehodey[2]

[1]Laboratoire d'Etudes Géophysiques et d'Océanographie Spatiale, LEGOS - UMR 5566 CNRS/CNES/IRD/UPS, Toulouse, France
[2]Collecte Localisation Satellite, CLS, Toulouse, France
[3]Mercator Ocean, Toulouse, France

Correspondence: Audrey Delpech (audreydelpech@wanadoo.fr)

Abstract. Micronekton – small marine pelagic organisms mostly in the size range 1-10 cm– is a key component of the ocean ecosystem, as it constitutes the main source of forage for all larger predators. Moreover, the mesopelagic component of micronekton that undergoes Diel Vertical Migration (DVM) likely plays a key role in the transfer and storage of CO_2 in the deep ocean: the so-called 'biological pump' mechanism. SEAPODYM-MTL is a spatially explicit dynamical model of micronekton. It simulates six functional groups of migrant and non-migrant micronekton, in the epipelagic and mesopelagic layers. Coefficients of energy transfer efficiency between primary production and each group are unknown. But they are essential as they control the predicted biomass. Since these coefficients are not directly measurable, a data assimilation method is used to estimate them. In this study, Observing System Simulation Experiments (OSSE) in the framework of twin experiments are used to test various observation networks at a global scale regarding energy transfer coefficients estimation. Observational networks show a variety of performances. It appears that environmental conditions are crucial to determine network efficiency. According to our study, ideal sampling areas are warm, non-dynamic and productive waters like the eastern side of tropical Oceans. These regions are found to reduce the error of estimated coefficients by 20% compared to cold and dynamic sampling regions. The results are discussed in term of interactions between physical and biological processes.

1 Introduction

Micronekton organisms are at the mid-trophic level of the ocean ecosystem and have thus a central role, as prey of all larger predator species and as a potential new resource in the blue economy (St John et al., 2016). Diel Vertical Migrations (DVM) characterizes a large biomass of the mesopelagic component of micronekton inhabiting the twilight zone (200-1000 m) of the world ocean. Through these daily migrations, the mesopelagic micronekton potentially contributes to a substantial transfer of atmospheric CO_2 to the deep ocean, after its metabolization by photosynthesis and export through the food chain. The understanding and quantification of this mechanism, called the 'biological pump', are crucial in the context of climate change (Zaret and Suffern, 1976; Benoit-Bird et al., 2009; Davison et al., 2013; Giering et al., 2014; Ariza et al., 2015). However, there is a lack of comprehensive dataset at global scale to properly estimate micronekton biomass and composition. The few existing estimates of global biomass of mesopelagic micronekton vary considerably between less than 1 and $\sim$ 20 Gt (Gjosaeter and

https://doi.org/10.5194/bg-2019-353
Preprint. Discussion started: 6 September 2019

Kawaguchi, 1980; Irigoien, 2014; Proud et al., 2018), so that micronekton has been compared to a "dark hole" in the studies of marine ecosystems (St John et al., 2016). Therefore, a priority is to develop the datasets, methods and models needed to simulate and quantify the dynamics and functional roles of these species' communities.

Observations and biomass estimations of micronekton rely traditionally on net sampling and active acoustic sampling (e.g., Handegard et al., 2009; Davison, 2011). Each method has limitations. Micronekton species can detect approaching fishing gears and part of them can move away to avoid the net. This phenomenon leads to biomass underestimation from net trawling (Kaartvedt et al., 2012). Conversely, acoustic signal intensity may overestimate biomass due to presence of organisms with strong acoustic target strength, e.g. many mesopelagic species but also siphonophores that have gas inclusion inducing strong resonance (Davison, 2011; Proud et al., 2017). Some organisms like squids, have both excellent skills to escape the trawl net and a low response to acoustic signal, making this component strongly underestimated with both methods. Progress are expected in the coming years thanks to the use of multiple acoustic frequencies associated to traditional net sampling and optical techniques (Kloser et al., 2016; Davison et al., 2015). More accurate biomass estimates should benefit from this combination of techniques and the developments of algorithms that can attribute acoustic signal to biological groups.

While these techniques of observation and methods of in situ estimates of biomass are progressing, new developments are also achieved in the modeling of ocean ecosystem including micronekton components. SEAPODYM (Spatial Ecosystem And POpulation Dynamics Model) is an eulerian ecosystem model that includes one lower- (zooplankton) and six mid-trophic (micronekton) functional groups, and detailed target fish populations (Lehodey et al., 1998, 2008). Given the structural importance of DVM, the functional groups are defined based on the daily migration behavior of organisms between three broad epi- and meso-pelagic bio-acoustic layers (Lehodey et al., 2010, 2015). The spatial dynamics of biomass in each group is driven by the ocean circulation, while a diffusion coefficient account for local random movements. The time of development and the natural mortality of organisms in the functional groups are linked to the temperature in the vertical layers inhabited during the day or night. These mechanisms are simulated with a system of advection-diffusion-reaction equations. Primary production is the source of energy distributed to each group according to a coefficient of transfer efficiency. Eleven parameters control the biological processes: a diffusion coefficient, six coefficients $(E'_i)_{i\in[\![1,6]\!]}$ of energy transfer from primary production toward each mid-trophic functional group and four parameters for the relationship between water temperature and time of development (mortality, recruitment) (Lehodey et al., 2010). The later four parameters were estimated from a compilation of data found in the scientific literature (Lehodey et al., 2010). Therefore, the largest uncertainty remains on the energy transfer efficiency coefficients, that control the total abundance of each functional group.

A method to estimate the model parameters has been developed using a Maximum Likelihood Estimation (MLE) approach (Senina et al., 2008). Its implementation is based on an adjoint technique (Errico, 1997) to iteratively optimize a cost function that represents the discrepancy between model outputs and observations. A first study has shown that this method can be used to estimate the parameters E'_i using relative ratios of observed acoustic signal and predicted biomass in the three vertical layers during daytime and nighttime (Lehodey et al., 2015). A single acoustic transect was used, with the strong assumption that acoustic signal and predicted biomass were directly proportional. While we can expect that improved estimates of micronekton biomass become available in the coming years, they will likely still require costly operations at sea. Therefore, it is useful to use

https://doi.org/10.5194/bg-2019-353
Preprint. Discussion started: 6 September 2019


Biogeosciences Discussions Open Access EGU

the model and its MLE approach to evaluate the potential that these observations contain for the model parameters estimation through Observing System Simulation Experiments (OSSE) (Arnold and Dey, 1986).

The objective of the present study is to characterize and identify the sampling regions, regarding oceanic variables, in which micronekton biomass observation gives the most useful information for the model energy transfer coefficients estimation. For this purpose, we use OSSE based on twin experiments. A set of synthetic observations is generated with SEAPODYM using a reference parameterization. Then, the set of parameter values is changed and an error is added to the forcing field in order to simulate more realistic conditions. The MLE is used to estimate the set of parameters from the set of synthetic observations. The difference between the reference and estimated parameters provides a metric to select the best sampling zones. A method based on the clustering (Jain et al., 1999) of oceanic variables (temperature, currents velocity, stratification and productivity) is presented to investigate the sensitivity of the parameters estimation to the oceanographic conditions of the observation regions. This method aims at determining which conditions are the most favorable for collecting observations in order to estimate the energy transfer efficiency coefficients.

The paper is organized as follows: Section 2 describes the model set-ups and forcings. The method developed to characterize regions of observations and the metrics used to evaluate the parameters estimation are detailed as well. Section 3 describes the outcome of the clustering method to define oceanographic regimes and synthesizes the main results of our estimation experiments. The results are then discussed in Section 4 in the light of biological and dynamical processes. Some applications and limitations of our study are also identified along with suggestions for possible future research.

2 Method

2.1 SEAPODYM-MTL and its configuration

SEAPODYM-MTL models six functional groups of micronekton in the epi- and upper and lower mesopelagic layers at a global scale. These layers encompass the upper 1000 m of the ocean, as observed from acoustic detection and net sampling. The euphotic depth (z_{eu}) is used to define the depth boundaries of the vertical layers. These boundaries are defined as follows: $z_1(x,y,t) = 1.5 \times z_{eu}(x,y,t)$, $z_2(x,y,t) = 4.5 \times z_{eu}(x,y,t)$, $z_3(x,y,t) = \min(10.5 \times z_{eu}(x,y,t), 1000)$, where z_{eu} is given in meters. The six functional groups are called (1) epi (for the organisms inhabiting permanently the epipelagic layer); (2) umeso (for the organisms inhabiting permanently the upper mesopelagic layer); (3) ummeso (for migrant-umeso, the organisms inhabiting the upper mesopelagic layer at day and the epipelagic layer at night); (4) lmeso (for the organisms inhabiting permanently the lower mesopelagic layer); (5) lmmeso (for migrant-lmeso, the organisms inhabiting the lower mesopelagic layer at day and the upper mesopelagic layer at night) and (6) lhmmeso (for highly migrant lmeso, the organisms inhabiting the lower mesopelagic layer at day and the epipelagic layer at night). The model is forced by current velocities, temperature and net primary production (see Appendix A for detailed equations).

This work is based on a ten-year (2006-2015) simulation of SEAPODYM-MTL, called hereafter the TRUTH simulation. Due to high computational demand, the original resolution of forcing fields (0.25°×week) has been degraded to 1°×month. Euphotic depth, horizontal velocity and temperature fields come from the ocean dynamical simulation FREEGLORYS2V4

https://doi.org/10.5194/bg-2019-353
Preprint. Discussion started: 6 September 2019

produced by Mercator-Ocean[1]. Temperature and horizontal velocity fields are depth-averaged over the water column of each three trophic layers ending with a three-layers forcings field set. Net primary production is estimated using the Vertically Generalized Production Model (VGPM) of Behrenfeld and Falkowski (1997) with satellite derived chlorophyll a concentration. This product is available at Ocean Productivity Home Page of the Oregon State University[2]. Initial conditions of SEAPODYM-MTL come from a two-years spin-up based on a monthly based climatology simulation in order to reach equilibrium. Reference values of SEAPODYM-MTL parameters in the TRUTH simulation are those published in Lehodey et al. (2010).

2.2 Clustering approach to characterize potential sampling regions

In this section we describe the method we use to select different observation sets for OSSE, based on environmental characteristics. We define the spatio-temporal discrete observable space Ω as the set of the $1°\times1°$ grid points belonging to SEAPODYM-MTL discrete domain. The characterization of each observation point relies on four indicators defined from the environmental variables: the depth-averaged temperature $\mathcal{T}$, a stratification index $\mathcal{S}$, the surface velocity norm $\mathcal{V}$ and a bloom index $\mathcal{B}$, for which different regimes of intensity are defined. The averaged temperature $\mathcal{T}$ over the water-column is defined as:

$$\mathcal{T}(x,y,t) = \frac{1}{3}(T_1(x,y,t) + T_2(x,y,t) + T_3(x,y,t)), \tag{1}$$

where T_k is the depth-averaged temperature over the k^{th} trophic layer of the model. The stratification index $\mathcal{S}$ is defined as the absolute difference of temperature between the surface and subsurface layers:

$$\mathcal{S}(x,y,t) = |T_2(x,y,t) - T_1(x,y,t)|. \tag{2}$$

The surface velocity norm $\mathcal{V}$ is defined as:

$$\mathcal{V}(x,y,t) = \sqrt{u_1^2(x,y,t) + v_1^2(x,y,t)}, \tag{3}$$

where u_1 and v_1 are respectively the zonal and meridional components of the depth-averaged velocity in the first layer of the model. The phytoplankton bloom index $\mathcal{B}$ is defined following Siegel et al. (2002) and Henson and Thomas (2007) as a Boolean: 1 for bloom regions and 0 for no bloom regions according to temporal variation relative to annual median threshold overshooting. More precisely, we define:

$$\mathcal{B}(x,y) = \begin{cases} 1 & \text{if there exists } t \text{ such that } \quad |PP(x,y,t) - \widetilde{PP}(x,y)| > 0.05 \times \widetilde{PP}(x,y), \\ 0 & \text{elsewhere.} \end{cases} \tag{4}$$

where $\widetilde{PP}(x,y)$ is the temporal median of the primary production $PP(x,y,t)$ at point (x,y). Note that contrary to the previous indicator variables, the bloom index does not depend on time. For each indicator variable $\mathcal{G} \in \{\mathcal{T},\mathcal{S},\mathcal{V},\mathcal{B}\}$ we define several ordered value-based *regimes*. The number of regimes together with regime boundary values are obtained by partitioning the set G_N of the values of the indicator variable $\mathcal{G}$ at N observable locations constituting an ensemble $S_N \subset \Omega$.

$$G_N = \{g_i = \mathcal{G}(X_i) \quad X_i \in S_N\}_{1\leq i\leq N}. \tag{5}$$

[1]https://www.mercator-ocean.fr/
[2]http://www.science.oregonstate.edu/ocean.productivity/

https://doi.org/10.5194/bg-2019-353
Preprint. Discussion started: 6 September 2019

The partition of G_N is computed using a k-mean clustering method (Kanungo et al., 2002) and the number of clusters is chosen according to the Elbow score (Kodinariya and Makwana, 2013; Tibshirani et al., 2001). The k-mean method leads to n clusters $(\Gamma_k)_{k\in[\![1,n]\!]}$ (called indicator variable regimes), that satisfy the following properties:

$$\begin{cases} \bigcup_{k=1}^{n}\Gamma_k = G_N \quad \text{and} \quad \bigcap_{k=1}^{n}\Gamma_k = \emptyset \\ \text{and} \\ \forall i \in [1,N], g_i \in \Gamma_k \quad \text{if} \quad k = \underset{l\in[1,n]}{\operatorname{argmin}} \|g_i - \mu_l\|, \end{cases} \tag{6}$$

where μ_l is the mean of values in Γ_l. Note that Γ_k depends on the variable $\mathcal{G}$. In the following, we explicit this dependence by denoting $\Gamma_k(\mathcal{G})$. We define a *configuration* as the intersection of a selection of regimes of given indicator variables. For $i \in [\![1,n_\mathcal{T}]\!]$, $j \in [\![1,n_\mathcal{S}]\!]$, $k \in [\![1,n_\mathcal{V}]\!]$ and $l \in [\![1,n_\mathcal{B}]\!]$, the configuration C is defined as:

$$C = \mathcal{T}_i \otimes \mathcal{S}_j \otimes \mathcal{V}_k \otimes \mathcal{B}_l = \Gamma_i(\mathcal{T}) \cap \Gamma_j(\mathcal{S}) \cap \Gamma_k(\mathcal{V}) \cap \Gamma_l(\mathcal{B}), \tag{7}$$

where $n_\mathcal{G}$ is the number of clusters for the indicator variable $\mathcal{G}$. For sake of simplicity we may also say that an observation point belongs to a configuration when the values of the indicator variables at this point belong to the corresponding regimes of the configuration. Each configuration corresponds to a subset $S_M \subset S_N$ of observable points.

2.3 Twin experiments

In this paper, the inverse model and MLE are used in the framework of twin experiments as in (Lehodey et al., 2015). A reference simulation (TRUTH) is generated from the reference configuration. The reference simulation is used to compute synthetic observations. The goal is to retrieve back the reference energy transfer coefficients of the six micronekton functional groups E'_i by assimilating the synthetic observations into a twin simulation of SEAPODYM. However, contrary to Lehodey 2015, an error is introduced to the reference forcing fields as input of the twin simulation. This is to consider more realistically the discrepancy between the real state of the ocean (represented here by the TRUTH simulation) during data collection and the simplified representation of these conditions by the ocean circulation model used for the parameter optimization. The twin simulation (TWIN) differs thus from the reference simulation (TRUTH) by the forcing fields and the coefficients E'_i. The reference forcing fields are perturbed with a white noise whose maximal amplitude is a fraction of the averaged fields. Let F be the considered forcing field and let $\overline{F}$ be its global average (in space and time), we define the perturbed field as

$$\widetilde{F}(x,y,t) = F(x,y,t) + \gamma(\alpha\overline{F}), \tag{8}$$

where $\alpha \in [0,1]$ is the amplitude of the perturbation and $\gamma \in [-1,1]$ is a uniformly distributed random number. The amplitude α is set to 0.1 for all experiments. The parameters E'_i are randomly sampled between 0 and 1. This *first guess* is used as initialization of the optimization scheme. We run each experiment several times with different random sampled first guess in order to ensure that the inverse model is not sensitive to the initial parameters. The set-up of the TRUTH and TWIN simulations are summarized in Table 1.

https://doi.org/10.5194/bg-2019-353
Preprint. Discussion started: 6 September 2019

In the framework of OSSE, we perform estimation experiments with different sets of fixed number ($N_e = 400$) of synthetic observation points. The synthetic observations are sampled in the different configurations constructed as explained in the previous section. Let M be the number of points in a given configuration. If $M < N_e$, we consider that the configuration is too singular to be relevant for our study and is ignored. If $M > N_e$ we randomly extract a sub-sample $S_{N_e} \subset S_M$ of observation points. In order to study the influence of one indicator at a time, we compare experiments for which the regime of the studied indicator varies and the regime of the other indicator variables remain fixed. In the following we call *primary variable* the studied indicator variable and *secondary variables* the ones whose regimes are fixed. For a given group of experiments, we check that the configurations are statistically comparable between each others by ensuring that the distribution of secondary variables are close enough between configurations (cf. marginal distribution plots in Section 3). If this not the case, they are not presented.

2.4 Estimation evaluation metrics

The estimation experiments are evaluated using three metrics: (i) the performance of the estimation, (ii) its accuracy and (iii) its convergence speed.

(i) The performance is measured with the mean relative error between the estimated coefficients and the reference coefficients as defined in Eq. 9:

$$E_r = \frac{1}{6}\sum_{i=1}^{6}\left|\frac{\widehat{E_i'} - E_i'}{E_i'}\right|. \tag{9}$$

(ii) The accuracy is measured by the residual value of the likelihood which provides a good estimate of the discrepancy between the estimated and observed biomass.

(iii) The convergence speed is measured by the iterations number of the optimization scheme.

The residual likelihood and iterations number metrics are provided by the Automatic Differentiation Model Builder (ADMB) algorithm (Fournier et al., 2012) that implements the MLE. Each metric provides different and independent information. For example, it is possible to obtain good performance and bad accuracy with an experiment that estimates correctly the energy transfer parameters for the different functional groups but over- or under-estimates the total amount of biomass. The performance is generally used to discriminate the different experiments since the aim of the study is to find the networks that better estimate energy transfer coefficients and thus directly minimize the error E_r (Eq. 9). However, the accuracy and precision of the experiment are discussed. The convergence is necessary to ensure that the optimization problem is well defined.

https://doi.org/10.5194/bg-2019-353
Preprint. Discussion started: 6 September 2019


Biogeosciences Discussions Open Access EGU

3 Results

3.1 Environmental regimes clustering

The number of points by regime defined for each environmental variable (Table 2) shows a large variability. Some regimes present a larger amount of observable points. For instance, the tropical temperature regime covers 31% of the observable points. Almost 50% of the observable show a weak stratification and only 10% of them have a positive bloom index or high velocities. When they are shown on a map (Figure 1) these regimes reproduce classical spatial patterns described in the scientific literature (Fieux and Webster, 2017). The regimes of the temperature variable ($\mathcal{T}$) show a latitudinal distribution. The polar regime ($\mathcal{T}_1$) is located south of the Polar front (Southern hemisphere) and in the Arctic Ocean. The subpolar regime is located between the Polar front and the South Tropical front (Southern Ocean), in the Labrador and Greenland Seas (North Atlantic) and in the Bering Sea (North Pacific). The temperate regime covers the subtropical zones of the Southern Atlantic, Indian and Pacific Oceans, located north of the South Tropical front, and extends as well in the eastern part of the Atlantic and Pacific Ocean. The tropical regime covers most of the tropical ocean and the Indian ocean. The regimes of the stratification variable ($\mathcal{S}$) are also structured according to the latitude as stratification depends on the temperature. The stratification decreases from the tropical oceans (where the surface waters are warm compared to the deep waters) to the pole (where the surface waters are almost as cold as the deep waters). The regimes of the velocity variable ($\mathcal{V}$) highlight the main energetic structures of the oceanic circulation. The high currents regime thus covers the intense jet-structured equatorial currents, the western boundary currents (the Gulf Stream in the Atlantic and the Kuroshio in the Pacific), the Agulhas current along the South Africa coast and the Antarctic Circumpolar Current in the Southern Ocean. The regimes of bloom index ($\mathcal{B}$) separate mostly the productive regions (North Atlantic and North Pacific, Southern Ocean, Eastern side of Tropical Atlantic, along the African coast) from the non productive regions (center of subtropical gyres mostly, as well as coastal regions of Arctic and Antarctic).

Based on this result, we construct and select configurations to conduct the OSSE (section 2.2). The choice of the configuration is limited by the number of observation points available in each of them. Among the 48 possible configurations, 22 of them are considered non-existent because they have less than 0.5% of all observable points. In addition, we study the influence of the primary variable by selecting only groups of configurations whose distributions along secondary variables are similar. This leads to a selection of 7 groups of experiments (Table 3). The first three groups of Experiments 1a-b, 1c-d and 1e-f are meant to study the influence of the velocity regimes $\mathcal{V}_1$ and $\mathcal{V}_2$. The group of Experiments 2a-d will be used to study the influence of the temperature regimes $\mathcal{T}_1$, $\mathcal{T}_2$, $\mathcal{T}_3$ and $\mathcal{T}_4$. The group Experiments 3a-c will be used to investigate the influence of the stratification index regimes $\mathcal{S}_1$, $\mathcal{S}_2$ and $\mathcal{S}_3$. Finally, Experiments 4a-b and 4c-d are used for the study the influence of the bloom index regimes $\mathcal{B}_1$ and $\mathcal{B}_2$.

https://doi.org/10.5194/bg-2019-353
Preprint. Discussion started: 6 September 2019


Biogeosciences Discussions Open Access EGU

3.2 Estimation performance with respect to environmental conditions

Table 3 shows the selected configurations for each experiment as well as their evaluation metrics. All experiments converged after 16 to 28 iterations. This confirms that the optimization problem is well defined. Since the number of iterations is partially dependent on the random initial first guess, it is not used as a criterion of discrimination between experiments.

3.2.1 Influence of the horizontal currents velocity

The influence of the currents velocity regimes (high currents system or low currents system) on the performance of the parameters estimation is studied considering three groups of experiments (Table 3, Exp. 1a to 1f). The observation points are randomly sampled in a subset of the considered configuration for which the primary variable is the currents velocity norm $\mathcal{V}$.

From these sets of experiments, it appears that the performance on the estimation of parameters decreases with the currents velocity at the observation point. This conclusion is valid whatever the regime of the secondary variables: either low or high temperatures, positive or null bloom index and weak or strong stratification (Table 3). Lower velocity reduces the error on the estimated energy transfer coefficients for functional groups that are impacted by currents in the epipelagic and upper mesopelagic layers. The currents decrease with depth and are almost uniform over the different regions in the lower mesopelagic layer (not shown). Consequently, the estimate of the parameters for the non migrant lower mesopelagic (lmeso) group is not sensitive to the regime of currents (Figure 2). Conversely, the estimation is the most sensitive for the epipelagic group, whose dynamics is entirely driven by the surface currents.

Note that the influence of low and high velocities is not explored for all secondary variable fixed regimes. Indeed, even with fixed regimes, the secondary variables distribution along observation points might not be statistically comparable between two experiments. This could lead to a potential bias introduced by a secondary variable, which is not the target of the study. For instance, the influence of velocity in a polar temperature regime can be investigated by comparing the configurations $C' = \mathcal{T}_1 \otimes \mathcal{S}_1 \otimes \mathcal{V}_1 \otimes \mathcal{B}_2$ and $C'' = \mathcal{T}_1 \otimes \mathcal{S}_1 \otimes \mathcal{V}_2 \otimes \mathcal{B}_2$. The corresponding twin experiments Exp. 1' (observations sampled in C') and Exp. 1" (observations sampled in C") estimate two sets of parameters whose relative distances to the target parameters are 48% and 10% respectively. Before concluding that observations in very cold (polar regimes) and highly dynamics waters improve the performance of the estimation, it is necessary to check the distributions of the observations along the secondary variables. The temperature shows the presence of a strong bias is (Figure 3). Therefore, despite it has been fixed to "polar regime", the temperature in configuration C' is on average lower (-0.7°C) than the temperature of configuration C" (2.1°C). Thus Experiments 1' and 1" measure correlatively the influence of the velocity and of the temperature. The lower velocities are coupled with lower temperatures and the higher velocities with higher temperatures. Therefore, it seems here that the difference observed in the temperature values of the two datasets has a stronger impact on the parameter estimation than the regime of currents.

In the following, although distribution along secondary variables are not always shown, they have always been used in the analysis to check that the results of twin experiments are not biased by this type of difference between the distributions of randomly selected datasets. Experiments with such cross-correlation between indicator variables are not presented.

https://doi.org/10.5194/bg-2019-353
Preprint. Discussion started: 6 September 2019

3.2.2 Influence of the temperature

In experiments 2a to 2d (Table 3), temperature is the primary variable, ranging from polar regime (Exp. 2a), to subpolar (Exp. 2b), temperate (Exp. 2c) and tropical (Exp. 2d) regimes. All other indicator variables (stratification, velocity and bloom index) are secondary variables that are set to weak, low and 1 respectively. Figure 5 shows that the distributions along the secondary variables of each configuration are close enough for the experiments to be compared, avoiding any risk of cross-correlation. The performance of the estimation increases with the temperature (Figure 4). The mean error on the parameter estimates decreases respectively from polar (Exp. 2a; 9.1%) to subpolar (Exp. 2b; 7%), temperate (Exp. 2c; 3%) and tropical (Exp. 2d; 1.4%) configurations (Table 3).

3.2.3 Influence of the vertical gradient of temperature

The influence of the stratification is investigated with a first set of three configurations combining tropical temperature regime, low velocity regime, null bloom index regime and three regimes of weak (Exp. 3a); intermediate (Exp. 3b) and strong (Exp. 3c) stratification. A marginal distribution plot of observation sets for all experiments (not shown) indicates that the three data sets differ only along the stratification variable (primary variable). The observation points display a temperature between $14°C$ and $17°C$, a velocity between 0 and 0.07 m s^{-1} and a null bloom index for each experiments. The performance decreases with the intensity of stratification (Figure 6 and Table 3). The mean error is: 3.5% for a weak stratification and a vertical gradient of about $0.4°C$ (Exp. 3a), 5.9% for an intermediate stratification with a gradient of about $5.9°C$ (Exp. 3b) and 8% for a strong stratification, around $11.7°C$ (Exp. 3c). A strong stratification seems to deteriorate the estimate for all migrant groups (Figure 6). These results are not specific to the choice of regimes for the secondary variables. The same kind of experiments were carried out in a temperate regime (not shown) and if the mean error on the estimated parameters were higher in average, the result does not change: a weak stratification always leads to a better estimation than a strong stratification. The comparison was not fully possible in other temperature or velocity regimes because these configurations are not sufficiently well represented (see Section 3.2.1 §2).

3.2.4 Influence of the primary production

In order to investigate the influence of the primary production on the performance of the estimation, we compare the results of estimation in configurations with different bloom index regimes (primary variable). Temperature, stratification index and velocity have been fixed (secondary variables) to subpolar, weak and low regimes respectively (Exp. 4a and 4b) and to tropical, strong and low for Exp. 4c and 4d. Distributions of the observation points along the secondary variables indicate that the experiments are not biased by secondary variables as the distributions present similar modes centered at $5°C$ for the temperature, at $0.5°C$ for the stratification index and at 0.04 m s^{-1} for the velocity (Exp. 1a and 1b) and at $15.5°C$, $11°$ and 0.05 m s^{-1} respectively for Exp. 4c and 4d (not shown).

Exp. 4a and 4b result both in an averaged error of 7% on the estimated parameters (Table 3). Exp. 4d (averaged error of 8%) gives a similar value as Exp. 4b. Indeed, not only the temperature is higher but also the vertical gradient of temperature. As

https://doi.org/10.5194/bg-2019-353
Preprint. Discussion started: 6 September 2019


Biogeosciences Discussions Open Access EGU

we concluded it from the two previous sections, the temperature improves the performance of the estimation when increasing and the gradient deteriorates the performance when increasing. So, the two effects might compensate in this case and result in a similar estimation. However, when considering bloom regions (Exp. 4c), the estimation error falls to 1.5% in average. In addition, this experiment estimates the energy transfer coefficients for migrant micronekton groups with less than 1% error (Figure 7).

3.3 Global map of parameters estimation errors

When considering all possible experiments, and given the fact that all these configurations are associated to specific locations and times, it is possible to represent a global map of averaged estimation error (Eq. 9). This map shows that on average, the error increases from the equator towards the poles (Figure 8). The lowest performances (errors $> 40\%$) are mostly found in the Arctic and Southern Ocean. Low performances are also found at some specific locations along the veins of the main currents. The signature of the Antarctic Circumpolar Current can be found in the Southern Ocean with error over 10%. Similarly, the signature of the North Atlantic Drift can be seen with a patch of high errors between Canada and Ireland (Figure 1c and 8). The patch of high errors in the North Pacific Ocean is however difficult to interpret. The equatorial regions show interesting patterns that are similar across the three oceans. In the vicinity of the equator, good performances are observed (mean error 2%). On both northern and southern sides of this low error band, the performance is degraded with errors reaching about 8%. The equatorial regions are characterized by strong currents and warm waters. As demonstrated above, these environmental features have antagonistic effects on the performance of the estimation. Therefore, a possible explanation of this distribution of errors is that water temperature is high enough to overcome the effect of currents velocity in the equatorial band, but when moving poleward, the temperature decreases cannot compensate anymore for the negative effect of currents which is still quite strong.

3.4 Testing realistic networks

The above experiments are based on random selection of observation points within a large subset. This technique was chosen to avoid any bias related to the temporal or spatial potential correlation of observation networks. However, sampling at sea is rarely randomly distributed and can generate correlations. To relax this strong assumption, we made twin experiments based on positions from real acoustic transects. Two regions are compared using positions data collected during the maintenance cruises of the PIRATA network of moorings in the Equatorial Atlantic Ocean (PIRATA[3]) and during research cruises of the British Antarctic Survey in Antarctic peninsula region (BAS[4]) (Figure 9).

The same forcing, method and initial parameterization were used with a random noise amplitude (α) increasing from 0 to 0.2. Subsets of $N_e = 400$ observations were selected along the transects to run the experiments. The resulting averaged relative error on the coefficients is shown as a function of the amplitude of perturbation (Figure 10a) for both networks. It appears that the estimation error increases with the amplitude of the error introduced on the forcing field. Also, whatever the

[3]http://www.brest.ird.fr/pirata/pirata
[4]https://www.bas.ac.uk/project/poets-wcb

https://doi.org/10.5194/bg-2019-353
Preprint. Discussion started: 6 September 2019

perturbation, the estimation error is always lower when using PIRATA observation networks than BAS observation networks. These results are fully consistent with the previous results indicating that networks located in tropical warm waters, as for PIRATA, give better estimates than the ones located in cold waters, as for the BAS (Figure 10b). The PIRATA network is thus a very promising observatory for the micronekton, especially since it already includes a complete set of various physical and biogeochemical parameters measurements (Foltz et al., 2019).

4 Discussion

The modeling of micronekton in SEAPODYM-MTL relies on relatively simple mechanisms with a few parameters and three fundamental environmental forcing variables: temperature, horizontal currents and primary production, that influence the dynamics of the model. They also influence the skills of the MLE to estimate its parameters, assuming that a reasonable set of accurate micronekton biomass values can be collected at sea. This study allowed characterizing oceanic configurations based on the four variables used to drive the model. Given the definition of micronekton functional groups based on the DVM behavior between vertical layers, the stratification can effectively result in important changes in the dynamics of micronekton and the resulting biomass distribution. Once defined with the clustering method, the configurations were used to run twin experiments allowing to identify which associated environmental conditions were the most favorable to the estimation of energy transfer efficiency coefficients of the model. We found that observations from warm temperature regions (such as temperate or tropical regions) were more effective than those from cold regions. The presence of a bloom at the location of observation also improves the performance of the estimation (especially in warm environment). Conversely, high temperature stratification and high intensity of currents are both found to deteriorate the estimation. Thus, at global scale, we found that the better conditions for the estimation of energy transfer coefficient are warm waters, low currents, low vertical temperature gradients and seasonally high primary production.

4.1 An interpretation of the performance in term of observability

The differences in the performance of parameter estimation can be interpreted in regard of the characteristic times of physical and biological processes. The parameters we want to estimate (E_i') control the energy transfer efficiency between the primary production (PP) and micronekton production (P) (Eq. A3; Appendix A). These parameters are thus directly related to the relative amount of P at age $\tau = 0$ in each functional group and we have:

$$E_i' = \frac{P_i(\tau = 0)}{cE_{pp} \int PP dz} \tag{10}$$

https://doi.org/10.5194/bg-2019-353
Preprint. Discussion started: 6 September 2019


Biogeosciences Discussions Open Access EGU

It is possible to rewrite the initial condition (Eq. A3) as a system of six equations involving the energy transfer coefficients.

$$\begin{cases} \rho_{1,d}(P_{|\tau=0}) = E'_1 \\ \rho_{1,n}(P_{|\tau=0}) = E'_1 + E'_3 + E'_6 \\ \rho_{2,d}(P_{|\tau=0}) = E'_2 + E'_3 \\ \rho_{2,n}(P_{|\tau=0}) = E'_2 + E'_4 \\ \rho_{3,d}(P_{|\tau=0}) = E'_4 + E'_5 + E'_6 \\ \rho_{3,n}(P_{|\tau=0}) = E'_4 \end{cases} \tag{11}$$

where $\rho_{K,\omega}(P_{|\tau=0})$ is the ratio of age 0 potential micronekton production in the layer $K \in \{1,2,3\}$, at the time of the day $\omega \in \{\text{day}, \text{night}\}$.

The micronekton predicted biomass in a given time and place (grid cell) results from two main mechanisms. First, the potential production evolves in time from age $\tau = 0$, and is redistributed by advection and diffusion until the recruitment time τ_r when it is transferred into biomass (B). Then, the biomass is built by accumulation of recruitment over time in each grid cell and is lost due to a temperature mortality rate, while the currents redistribute the biomass. The observations are the relative amount of biomass in each layer, i.e. the ratios of biomass $\rho_{K,\omega}(B_{|t=t^o})$ (Eq. A5), where t^o is the time at which the observation is collected. Therefore, the observation will be as close as the energy transfer parameters we want to estimate if $\rho_{K,\omega}(B_{|t=t^o})$ is close to $\rho_{K,\omega}(P_{|\tau=0})$. This requires the integrated mixing of biomass during the elapsed time between the age 0 of potential production and the time of observation (i.e.. at least the recruitment time) being as weak as possible. This can be achieved in different ways: (i) either the currents are weak so that the advective mixing is also weak (but still the diffusive mixing will remain); (ii) Or the temperature is high, leading to a short recruitment time with reduced period of transport and redistribution. These two mechanisms can explain why warm temperatures and weak currents were found to improve the estimations compared to cold temperatures or high velocities (Sections 3.2.1 and 3.2.2). An additional effect of warm temperature is to induce a higher mortality rate. When warm waters are combined with high primary production (e.g. the equatorial upwelling region), there is a rapid turnover of biomass and relative ratios of biomass by layer closer to the initial ratio of energy transfer efficiency coefficients. Conversely, at cold temperature, the mortality rate is lower; biomass is accumulated from recruitment events with a more distant origin and carries with it the integrated mixing and the perturbed ratio structures. This can explain why, at warm temperature, high productivity was needed for a better estimation (section 3.2.4). A side effect is that if temperature is not homogeneous across layers, then the mortality rate λ will differ for each functional group, depending on the layers it inhabits. This will be an additional driver of perturbation on the observed ratios of biomass. This is consistent with the result that a strong thermal stratification degrades the performance of estimation (section 3.2.3).

An observation will thus be the most effective for the estimation of parameters if it carries the information of the initial distribution of primary production into functional groups. This is the case if the biomass is renewed quickly enough compared to the time it takes for the currents and diffusive coefficient to mix it. This condition can be seen in term of equilibrium between the biological processes (production, recruitment and mortality) and the physical processes (advection and diffusion). In other words, for an observation to be effective for the estimation and not to introduce errors, it is necessary that the characteristics

https://doi.org/10.5194/bg-2019-353
Preprint. Discussion started: 6 September 2019

time governing biological processes (τ_β) is shorter than the one governing physical processes (τ_ϕ) at the location of the observation : $\tau_\beta \ll \tau_\phi$.

This interpretation highlights the problem of observability of the parameters E_i' from the measurements $\rho_{K,\Omega}(B)$. The parameters are directly observable at the age $\tau = 0$ of the primary production, but the measurements and the information we can get on the system are available only after a time τ_r. The observability will then be the better if the observable variables have not changed too much during the time τ_r (short τ_r, slow ocean dynamics). This is intrinsically linked to governing equations of the system (Eq. A1-A3) and therefore should not be dependent of the framework of the study.

4.2 Towards eco-regionalization ?

The clustering approach we propose allowed identifying oceanic regions that provide optimal oceanic characteristics for our parameters estimation by discriminating regions where the distribution of biomass is driven by physical processes from regions where it is driven by biological processes. It gives an essential information on the optimal regions for implementing observation networks. This could be seen as a new definition of eco-regions based on similar ecosystem structuring dynamics. The definition of ocean eco-regions has been proposed based on various criteria (Emery, 1986; Longhurst, 1995; Spalding et al., 2012; Fay and McKinley, 2014; Sutton et al., 2017; Proud et al., 2017). A convergence from these different approaches to identify regions characterized by homogeneous mesopelagic species communities would be of great interest to facilitate the modeling and biomass estimate of these components. Acoustic observation models could be developed and validated at the scale of these regions. Then, the observation models integrated to ecosystem and micronekton models as the one used here, would serve to convert their predicted biomass into acoustic signal to be directly compared to all acoustic observations collected in the selected region. This approach would allow to account for (and estimate) the sources of biases and errors linked to acoustic observations directly in the data assimilation scheme.

4.3 Limitations and perspectives

We have chosen to model the error between the true state of the ocean and the twin simulation by adding a white noise perturbation to the forcings. This method has been chosen to introduce a spatial homogeneous error to avoid any bias. A random noise ensures that the results obtained in different location are directly comparable. Nevertheless, other approaches would be interesting to explore. For instance, implementing an error proportional to the deviation of the climatological field should be more realistic because it would be based on the natural and intrinsic variability of the ocean. In addition to the uncertainty on ocean models outputs, other sources of uncertainties remain to be explored to progress toward more realistic estimation experiments. For instance, we considered that the observation operator (Eq. A5) is perfect but field observations are always tainted by errors. The micronekton biomass estimates at sea require a chain of extrapolation and corrections to account for the sampling gear selectivity and the portion of water layer sampled. For acoustic data, many factors need to be considered sources of potential error: the correction with depth, the target strength of species, the intercalibration between instruments and the signal processing methods (Handegard et al., 2009, 2012; Kaartvedt et al., 2012; Proud et al., 2018). This is an important research domain that requires to combine multiple observation systems, including new emerging technologies

https://doi.org/10.5194/bg-2019-353
Preprint. Discussion started: 6 September 2019

as broadband acoustic, optical imagery and environmental DNA to reduce overall bias in estimates of micronekton biomass (e.g., Kloser et al., 2016) and use those estimates to assess, initiate and assimilate into ecosystem models. Finally, the results of the clustering approach need to be confirmed with other ocean circulation model outputs, especially at higher resolution to check the impact of the mesoscale activity on the definition of optimal regions for energy transfer efficiency estimation.

5 Conclusions

Understanding and modelling marine ecosystem dynamics is considerably challenging. It generally requires sophisticated models relying on a certain number of parameterized physical and biological processes. SEAPODYM-MTL provides a parsimonious approach with only a few parameters and a MLE to estimates these parameters from observations. The energy transfer efficiency coefficients directly control the biomass of micronekton functional groups, including those that undergo DVM and contribute to the sequestration of carbon dioxide into the deep ocean (Davison et al., 2013; Giering et al., 2014; Ariza et al., 2015). Therefore, a correct assessment of energy transfer coefficients is crucial for climate studies. Given the high cost of observation at sea, the design of optimal observation networks through simulation experiments (OSSE) is a valuable approach before the deployment of observing platforms. This study provides a methodology for implementing such an observation network, based on the definition of oceanic regions using only four variables: the depth-averaged temperature, a thermal stratification index, the surface currents velocity norm and a bloom index. Twin experiments that were conducted in these regions with random sampling or based on realistic existing networks have shown that the quality of the estimation of the energy transfer efficiency coefficients is mainly linked to environmental conditions. The optimal combination of environmental factors is found for productive, warm and moderately stratified waters, with weak dynamics, such as the eastern side of the tropical Oceans. An interpretation in term of balance between characteristic times of biological and physical processes has been proposed to explain these results. In a future study, in addition to test the impact of introducing noises in the observations, the same approach could be used to directly estimate also the model parameters that control the relationship between the water temperature and the time of development of micronekton organisms.

Appendix A: SEAPODYM-MTL underlying equations

SEAPODYM-MTL is based on a system of advection-diffusion-reaction equations for each functional group i, $i \in [\![1,6]\!]$, involving two state variables: the potential production P_i (expressed in gramm of wet weight by squared meters by day, $\mathrm{gWWm^{-2}d^{-1}}$) and the biomass B_i (expressed in gramm of wet weight by squared meters, $\mathrm{gWWm^{-2}}$):

$$\frac{\partial B_i}{\partial t} = -\left(\frac{\partial}{\partial x}(uB_i) + \frac{\partial}{\partial y}(vB_i)\right) + D\left(\frac{\partial^2 B_i}{\partial x^2} + \frac{\partial^2 B_i}{\partial y^2}\right) - \lambda(T)B_i + P_i(\tau_r(T)), \tag{A1}$$

$$\frac{\partial P_i}{\partial t} = -\left(\frac{\partial}{\partial x}(uP_i) + \frac{\partial}{\partial y}(vP_i)\right) + D\left(\frac{\partial^2 P_i}{\partial x^2} + \frac{\partial^2 P_i}{\partial y^2}\right) - \frac{\partial P_i}{\partial \tau}, \tag{A2}$$

https://doi.org/10.5194/bg-2019-353
Preprint. Discussion started: 6 September 2019

where x, y, t and τ are the variables for space, time and age respectively. u, v (ms^{-1}) and T ($^{\circ}\mathrm{C}$) are the currents velocities and temperature respectively. These variables are integrated over each layer K, $K \in [\![1,3]\!]$ and weighted by the time each functional group i spends in the layer. D is the diffusion coefficient accounting for both the physical diffusion and the ability of micronekton organisms to swim short distances. τ_r (days) is the recruitment coefficient corresponding to the age for which the potential production converts into biomass of micronekton. λ (days^{-1}) is the mortality coefficient which accounts for natural mortality. Note that these two last parameters depend on the temperature.

The initial conditions for this system are :

$$B_i(t=0) = B_0, \quad P_i(t=0) = P_0, \tag{A3}$$

$$P_i(\tau=0) = cE_i' E_{pp} \int_{z_3}^{0} PP\, dz, \tag{A4}$$

where B_0 and P_0 are obtained by spinup, PP (in milimol of carbon per cubic meters per day, $\mathrm{mmolCm}^{-3}\mathrm{d}^{-1}$) is the net primary production, E_{pp} (adimensional) is the total energy transfer from the primary production to the mid-trophic level, E_i' (adimensional) is the distribution of this energy into the different functional groups, c is the conversion coefficient between mmolC and gWW and $z_3 = min(10.5 \times z_{eu}, 1000)$, z_{eu} the euphotic depth (in meters).

A module estimates SEAPODYM-MTL parameters by a variational data assimilation method : a Maximum Likelihood Estimation (MLE) (Senina et al., 2008). This method minimizes a cost function (the likelihood) that measures the distance between the biomass predicted by the model and the observed biomass. As the model outputs and the observations are not directly comparable, they are transformed with an observation model operator $\mathcal{H}$. $\mathcal{H}$ is defined for each layer K as :

$$\mathcal{H} \quad : \quad B \quad \mapsto \quad \rho_{K,\omega} = \frac{\sum_{i|K(i,\omega)=K} B_i}{\sum_{i=1}^{6} B_i} \tag{A5}$$

where $K(i,\omega)$ denotes the layer that the functional group number i occupies at the time of the day ω. $\mathcal{H}$ gives for each layer the relative amount of biomass that we call *ratio* (Lehodey et al., 2015).

The gradient of the likelihood function is computed using the adjoint state method. The parameters are then estimated using a quasi-Newton algorithm implemented by the Automatic Differenciation Model Builder (ADMB) algorithm (Fournier et al., 2012). SEAPODYM-MTL and the exact formulation of the cost function are described in detail in Lehodey et al. (2015).

Author contributions. AD designed the method, conducted the study ,analyzed the results and wrote the original manuscript. AC and OT contributed to the development of the parameter estimation component of SEAPODYM-MTL and helped designing the method. OT prepared the forcing fields, provided a technical support and a redaction support. PL coordinated the AtlantOS activity at CLS and contributed to the design of the study, the analysis of results and the redaction.

Competing interests. The authors declare that they have no conflict of interest.

https://doi.org/10.5194/bg-2019-353
Preprint. Discussion started: 6 September 2019

Acknowledgements. This publication has been developed in cooperation with the European Union's Horizon 2020 research and innovation project AtlantOS (633211). The authors thank the Groupe Mission Mercator Coriolis (Mercator Ocean) for providing the ocean general circulation model FREEGLORYS2V4 reanalysis and Jacques Stum and Benoit Tranchant at Collecte Localisation Satellite for processing satellite primary production and ocean reanalysis data. We also thank Arnaud Bertrand and Jérémie Habasque from the Institut de Recherche pour le Développement and Sophie Fielding from the British Antarctic Survey for making the cruise trajectories available.

https://doi.org/10.5194/bg-2019-353
Preprint. Discussion started: 6 September 2019

References

Ariza, A., Garijo, J., Landeira, J., Bordes, F., and Hernández-León, S.: Migrant biomass and respiratory carbon flux by zooplankton and micronekton in the subtropical northeast Atlantic Ocean (Canary Islands), Progress in Oceanography, 134, 330–342, 2015.

Arnold, C. P. and Dey, C. H.: Observing-systems simulation experiments: Past, present, and future, Bulletin of the American Meteorological Society, 67, 687–695, 1986.

Behrenfeld, M. and Falkowski, P.: Photosynthetic rates derived from satellite-based chlorophyll concentration, Limnology and Oceanography, 42, 1–20, 1997.

Benoit-Bird, K., Au, W., and Wisdoma, D.: Nocturnal light and lunar cycle effects on diel migration of micronekton, Limnology and Oceanography, 54, 1789–1800, 2009.

Davison, P.: The specific gravity of mesopelagic fish from the northeastern pacific ocean and its implications for acoustic backscatter., Journal of Marine Sciences, 68, 2064–2074, 2011.

Davison, P., Checkley Jr, D., Koslow, J., and Barlow, J.: Carbon export mediated by mesopelagic fishes in the northeast Pacific Ocean, Progress in Oceanography, 116, 14–30, 2013.

Davison, P. C., Koslow, J. A., and Kloser, R. J.: Acoustic biomass estimation of mesopelagic fish: backscattering from individuals, populations, and communities, ICES Journal of Marine Science, 72, 1413–1424, 2015.

Emery, W. J.: Global water masses: summary and review, Oceanologica acta, 9, 383–391, 1986.

Errico, R. M.: What is an adjoint model?, Bulletin of the American Meteorological Society, 78, 2577–2592, 1997.

Fay, A. and McKinley, G.: Global open-ocean biomes: mean and temporal variability, Earth System Science Data, 6, 273–284, 2014.

Fieux, M. and Webster, F.: The planetary ocean, Current natural sciences, EDP sciences, 2017.

Foltz, G. R., Brandt, P., Richter, I., Rodríguez-Fonseca, B., Hernandez, F., Dengler, M., Rodrigues, R. R., Schmidt, J. O., Yu, L., Lefevre, N., et al.: The tropical atlantic observing system, Frontiers in Marine Science, 6, 2019.

Fournier, D. A., Skaug, H. J., Ancheta, J., Ianelli, J., Magnusson, A., Maunder, M. N., Nielsen, A., and Sibert, J.: AD Model Builder: using automatic differentiation for statistical inference of highly parameterized complex nonlinear models, Optimization Methods and Software, 27, 233–249, 2012.

Giering, S., Sanders, R., Lampitt, R., Anderson, T., Tamburini, C., and Boutif, M.: Reconciliation of the carbon budgetin the ocean's twilight zone., Nature, 507, 480–483, 2014.

Gjosaeter, J. and Kawaguchi, K.: A review of the world ressources of mesopelagic fishes., Food Agriculture Org, pp. 193–199, 1980.

Handegard, N., Du Buisson, L., Brehmer, P., Chalmers, S., De Robertis, A., Huse, G., and Kloser, R.: Acoustic estimates of mesopelagic fish: as clear as day and night?, Journal of Marine Sciences, 66, 1310–1317, 2009.

Handegard, N., Du Buisson, L., Brehmer, P., Chalmers, S., De Robertis, A., Huse, G., and Kloser, R.: Towards an acoustic-based coupled observation and modelling system for monitoring and predicting ecosystem dynamics of the open ocean., Fish and Fisheries, 2012.

Henson, S. A. and Thomas, A. C.: Interannual variability in timing of bloom initiation in the California Current System, Journal of Geophysical Research: Oceans, 112, 2007.

Irigoien, X.: Large mesopelagic fishes biomass and trophic efficiency in the open ocean., Nature Communication, 5, 2014.

Jain, A. K., Murty, M. N., and Flynn, P. J.: Data clustering: a review, ACM computing surveys (CSUR), 31, 264–323, 1999.

Kaartvedt, S., Staby, A., and Aksnes, D. L.: Efficient trawl avoidance by mesopelagic fishes causes large underestimation of their biomass, Marine Ecology Progress Series, 456, 1–6, 2012.

https://doi.org/10.5194/bg-2019-353
Preprint. Discussion started: 6 September 2019

Kanungo, T., Mount, D. M., Netanyahu, N. S., Piatko, C. D., Silverman, R., and Wu, A. Y.: An efficient k-means clustering algorithm: Analysis and implementation, IEEE Transactions on Pattern Analysis & Machine Intelligence, pp. 881–892, 2002.

Kloser, R. J., Ryan, T. E., Keith, G., and Gershwin, L.: Deep-scattering layer, gas-bladder density, and size estimates using a two-frequency acoustic and optical probe, ICES Journal of Marine Science, 73, 2037–2048, 2016.

Kodinariya, T. M. and Makwana, P. R.: Review on determining number of Cluster in K-Means Clustering, International Journal, 1, 90–95, 2013.

Lehodey, P., Andre, J.-M., Bertignac, M., Hampton, J., Stoens, A., Menkès, C., Mémery, L., and Grima, N.: Predicting skipjack tuna forage distributions in the equatorial Pacific using a coupled dynamical bio-geochemical model, Fisheries Oceanography, 7, 317–325, 1998.

Lehodey, P., Sennina, I., and Murtugudde: A spatial ecosystem and population dynamics model - modeling of tuna and tuna-like population., Progress in Oceanography, 78, 304–318, 2008.

Lehodey, P., Murtugudde, R., and Senina, I.: Bridging the gap from ocean models to population dynamics of large marine predators : A model of mid-trophic functional groups., Progress in Oceanography, 84, 69–84, 2010.

Lehodey, P., Conchon, A., Senina, I., Domokos, R., Calmettes, B., Jouano, J., Hernandez, O., and Kloser, R.: Optimization of a micronekton model with acoustic data, Journal of Marine Science, 2015.

Longhurst, A.: Seasonal cycles of pelagic production and consumption, Progress in oceanography, 36, 77–167, 1995.

Proud, R., Cox, M. J., and Brierley, A. S.: Biogeography of the global ocean's mesopelagic zone, Current Biology, 27, 113–119, 2017.

Proud, R., Handegard, N. O., Kloser, R. J., Cox, M. J., and Brierley, A. S.: From siphonophores to deep scattering layers: uncertainty ranges for the estimation of global mesopelagic fish biomass, ICES Journal of Marine science, 76, 718–733, 2018.

Senina, I., Silbert, J., and Lehodey, P.: Parameter estimation for basin-scale ecosytem-linked population models of large pelagic predators : Application to skipjack tuna., Progress in Oceanography, 2008.

Siegel, D., Doney, S., and Yoder, J.: The North Atlantic spring phytoplankton bloom and Sverdrup's critical depth hypothesis, science, 296, 730–733, 2002.

Silverman, B. W.: Density estimation for statistics and data analysis, Routledge, 2018.

Spalding, M. D., Agostini, V. N., Rice, J., and Grant, S. M.: Pelagic provinces of the world: a biogeographic classification of the world's surface pelagic waters, Ocean & Coastal Management, 60, 19–30, 2012.

St John, M. A., Borja, A., Chust, G., Heath, M., Grigorov, I., Mariani, P., Martin, A. P., and Santos, R. S.: A dark hole in our understanding of marine ecosystems and their services: perspectives from the mesopelagic community, Frontiers in Marine Science, 3, 31, 2016.

Sutton, T. T., Clark, M. R., Dunn, D. C., Halpin, P. N., Rogers, A. D., Guinotte, J., Bograd, S. J., Angel, M. V., Perez, J. A. A., Wishner, K., et al.: A global biogeographic classification of the mesopelagic zone, Deep Sea Research Part I: Oceanographic Research Papers, 126, 85–102, 2017.

Tibshirani, R., Walther, G., and Hastie, T.: Estimating the number of clusters in a data set via the gap statistic, Journal of the Royal Statistical Society: Series B (Statistical Methodology), 63, 411–423, 2001.

Zaret, T. and Suffern, J.: Vertical migration in zooplankton as a predator avoidance mechanism, Limnology and Oceanography, 21, 804–816, 1976.

https://doi.org/10.5194/bg-2019-353
Preprint. Discussion started: 6 September 2019

Biogeosciences Discussions Open Access EGU

Table 1. SEAPODYM-MTL parameters used for the two different simulation TRUTH and TWIN. E is the energy transferred by net primary production to intermediate trophic levels, λ is the mortality coefficient, τ_r is the minimum age to be recruited in the mid-trophic functional population, D is the diffusion rate that models the random dispersal movement of organisms. $E'_i, i \in [\![1,6]\!]$ are the redistribution energy transfer coefficients to the 6 components of the micronekton population. The parametrization of the TRUTH simulation is called the reference parametrization and is taken from Lehodey et al. (2010).

Simulation	$1/\lambda$ (d)	τ_r (d)	D ($\mathrm{NM^2 d^{-1}}$)	E	E_1	E'_2	E'_3	E'_4	E'_5	E'_6	Forcing
TRUTH	2109	527	15	0.0042	0.17	0.10	0.22	0.18	0.13	0.20	F
TWIN	2109	527	15	0.0042	——— first guess ———						$\widetilde{F}$ (Eq. 8)

https://doi.org/10.5194/bg-2019-353
Preprint. Discussion started: 6 September 2019

Biogeosciences
Discussions
Open Access
EGU

Table 2. Outcome of the clustering method (Section 2.2). For each indicator variable (Temperature $\mathcal{T}$, Stratification $\mathcal{S}$, Velocity $\mathcal{V}$ and Bloom Index $\mathcal{B}$), the number n of clusters, the center and size (# observable) of each cluster (regimes) are given, as well as the proportion of all observable point it represents.

	Temperature ($\mathcal{T}$; $n=4$)				Stratification ($\mathcal{S}$; $n=3$)			Velocity ($\mathcal{V}$; $n=2$)		Bloom Index ($\mathcal{B}$; $n=2$)	
Regimes	$\mathcal{T}_1$	$\mathcal{T}_2$	$\mathcal{T}_3$	$\mathcal{T}_4$	$\mathcal{S}_1$	$\mathcal{S}_2$	$\mathcal{S}_3$	$\mathcal{V}_1$	$\mathcal{V}_2$	$\mathcal{B}_1$	$\mathcal{B}_2$
Regime names of $\Gamma_k(\mathcal{G})$, $k \in [\![1,n]\!]$	**polar**	**subpolar**	**temperate**	**tropical**	**weak**	**inter.**	**strong**	**low**	**high**	**bloom**	**no bloom**
Cluster center	0.4°C	6.4°C	12.6°C	16.3°C	0.4°C	5.9°C	11.7°C	0.05 ms^{-1}	0.3 ms^{-1}	74.6 $\mathrm{mmolCm}^{-2}\mathrm{d}^{-1}$	18.4 $\mathrm{mmolCm}^{-2}\mathrm{d}^{-1}$
# Observable in cluster	1106695	658105	1115102	1300298	2084302	1212945	882949	3698826	481367	449545	3730655
Proportion	26.5%	15.7%	26.7%	31.1%	49.8%	29.0%	21.1%	88.5%	11.5%	10.8%	89.2%

https://doi.org/10.5194/bg-2019-353
Preprint. Discussion started: 6 September 2019

Biogeosciences Discussions Open Access EGU

Table 3. Experiment table. List of experiments, their corresponding configurations and the evaluation diagnostics: mean relative error on the coefficients, residual likelihood and number of iterations. The section in which each of these experiment is discribed is given in the last column.

Experiment	Configuration	E_r (Eq. 9)	Residual Likelihood	# Iterations	Section
1a	$\mathcal{T}_2 \otimes \mathcal{S}_1 \otimes \mathcal{V}_1 \otimes \mathcal{B}_2$	7.0%	0.9	28	3.2.1
1b	$\mathcal{T}_2 \otimes \mathcal{S}_1 \otimes \mathcal{V}_2 \otimes \mathcal{B}_2$	9.7%	0.5	21	
1c	$\mathcal{T}_3 \otimes \mathcal{S}_1 \otimes \mathcal{V}_1 \otimes \mathcal{B}_1$	3.1%	0.5	24	
1d	$\mathcal{T}_3 \otimes \mathcal{S}_1 \otimes \mathcal{V}_2 \otimes \mathcal{B}_1$	8.3%	1.5	23	
1e	$\mathcal{T}_4 \otimes \mathcal{S}_3 \otimes \mathcal{V}_1 \otimes \mathcal{B}_1$	1.5%	1.1	16	
1f	$\mathcal{T}_4 \otimes \mathcal{S}_3 \otimes \mathcal{V}_2 \otimes \mathcal{B}_1$	8.5%	1.2	18	
2a	$\mathcal{T}_1 \otimes \mathcal{S}_1 \otimes \mathcal{V}_1 \otimes \mathcal{B}_1$	9.1%	1.7	19	3.2.2
2b	$\mathcal{T}_2 \otimes \mathcal{S}_1 \otimes \mathcal{V}_1 \otimes \mathcal{B}_1$	7.0%	0.6	26	
2c	$\mathcal{T}_3 \otimes \mathcal{S}_1 \otimes \mathcal{V}_1 \otimes \mathcal{B}_1$	3.1%	1.3	20	
2d	$\mathcal{T}_4 \otimes \mathcal{S}_1 \otimes \mathcal{V}_1 \otimes \mathcal{B}_1$	1.4%	0.6	22	
3a	$\mathcal{T}_4 \otimes \mathcal{S}_1 \otimes \mathcal{V}_1 \otimes \mathcal{B}_2$	3.5%	0.7	21	3.2.3
3b	$\mathcal{T}_4 \otimes \mathcal{S}_2 \otimes \mathcal{V}_1 \otimes \mathcal{B}_2$	5.9%	0.8	25	
3c	$\mathcal{T}_4 \otimes \mathcal{S}_3 \otimes \mathcal{V}_1 \otimes \mathcal{B}_2$	8.0%	1.1	21	
4a	$\mathcal{T}_2 \otimes \mathcal{S}_1 \otimes \mathcal{V}_1 \otimes \mathcal{B}_1$	7.0%	0.6	26	3.2.4
4b	$\mathcal{T}_2 \otimes \mathcal{S}_1 \otimes \mathcal{V}_1 \otimes \mathcal{B}_2$	7.0%	0.9	28	
4c	$\mathcal{T}_4 \otimes \mathcal{S}_3 \otimes \mathcal{V}_1 \otimes \mathcal{B}_1$	1.5%	0.6	22	
4d	$\mathcal{T}_4 \otimes \mathcal{S}_3 \otimes \mathcal{V}_1 \otimes \mathcal{B}_2$	8.0%	0.8	21	

https://doi.org/10.5194/bg-2019-353
Preprint. Discussion started: 6 September 2019

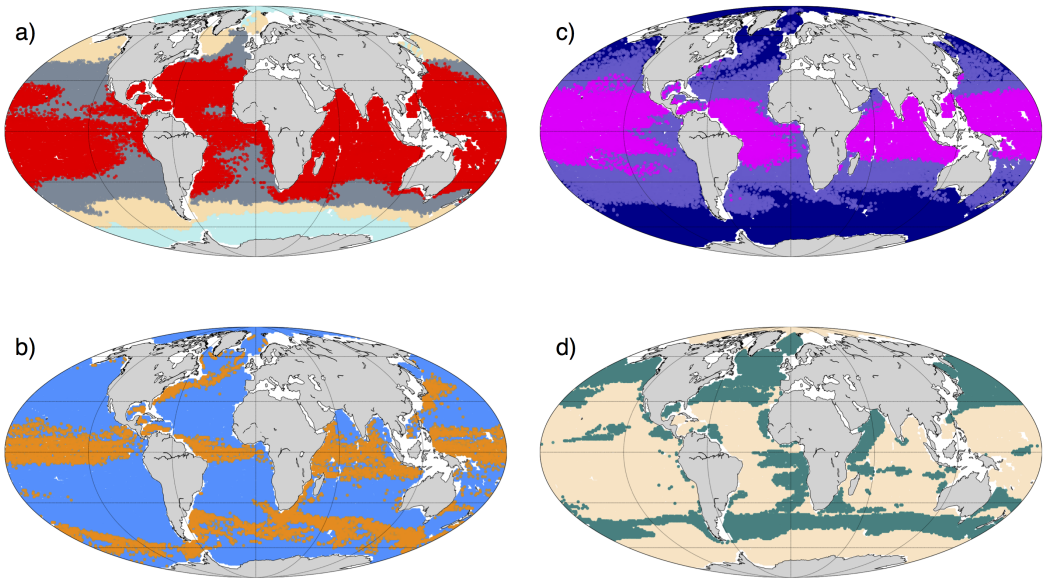

Figure 1. Spatial division of the different regimes. **(a) Temperature** : polar (pale blue), subpolar (yellow), temperate (gray), tropical (red). **(b) Stratification** : weak (dark blue), intermediate (purple), strong (magenta). **(c) Currents Velocities** : low (blue), high (orange). **(d) Bloom Index** : bloom (green), no bloom (beige). Each point of the subset S_N has been plotted at its spatial location with a color corresponding to the regime it belongs to. A transparency factor has been applied in order to account for the temporal fluctuation of regimes (a given point may belongs to different regimes over time). The resulting color on the map corresponds to the most frequent regime the corresponding point belongs to.

https://doi.org/10.5194/bg-2019-353
Preprint. Discussion started: 6 September 2019

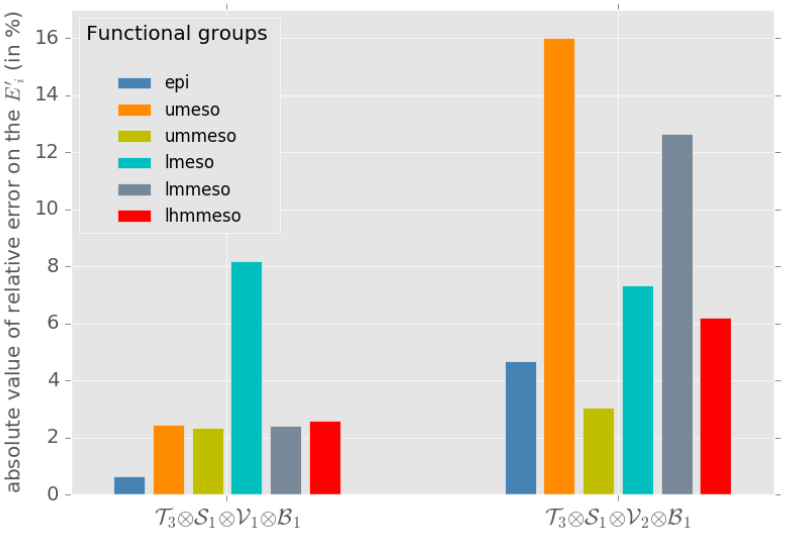

Figure 2. Mean relative error (E_r in %, Eq. 9) on each E'_i coefficients. Exp. 1c and 1d : high vs low velocities in temperate temperatures, weak stratification and bloom regimes.

https://doi.org/10.5194/bg-2019-353
Preprint. Discussion started: 6 September 2019

Biogeosciences
Discussions
Open Access
EGU

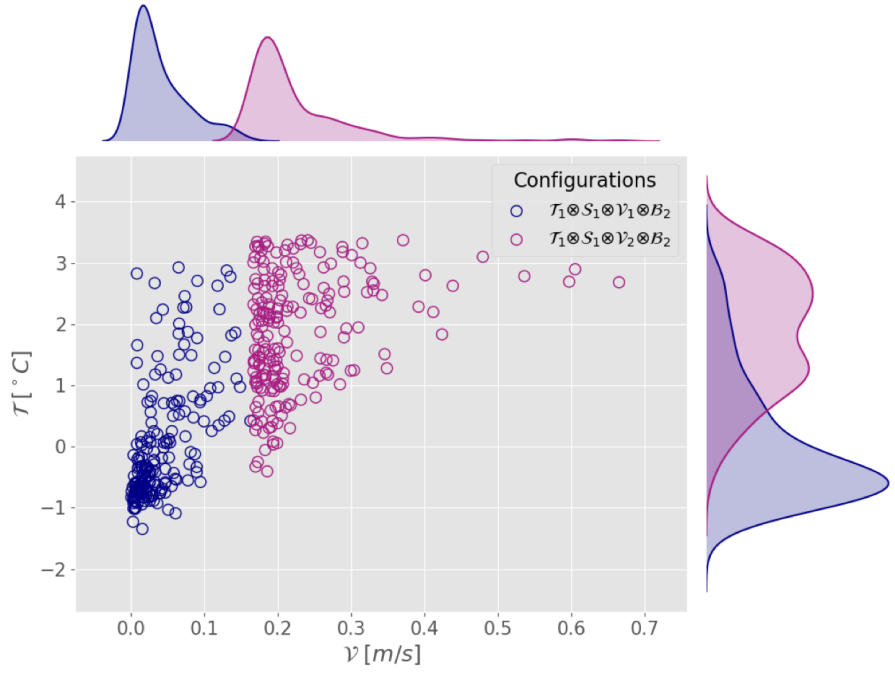

Figure 3. Scatter plot and marginal distribution from kernel density estimation (Silverman, 2018) in the plane ($\mathcal{V}$,$\mathcal{T}$) of observation points used in Exp. 1' and 1" generated by random sampling in configurations $C' = \mathcal{T}_1 \otimes \mathcal{S}_1 \otimes \mathcal{V}_1 \otimes \mathcal{B}_2$ and $C'' = \mathcal{T}_1 \otimes \mathcal{S}_1 \otimes \mathcal{V}_2 \otimes \mathcal{B}_2$.

https://doi.org/10.5194/bg-2019-353
Preprint. Discussion started: 6 September 2019

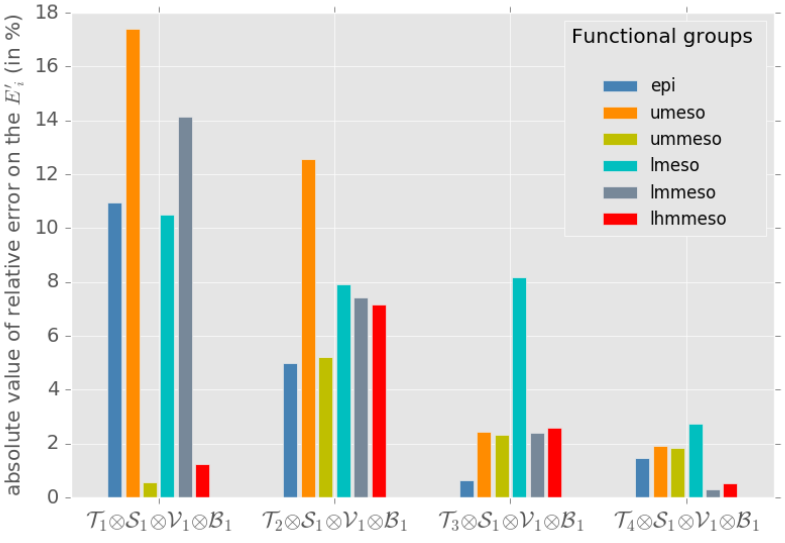

Figure 4. Mean relative error (E_r in %, Eq. 9) on each E'_i coefficients for Exp. 2a, 2b, 2c and 2d : polar vs subpolar vs temperate vs tropical temperatures in weak stratification, low velocity and bloom regimes.

https://doi.org/10.5194/bg-2019-353
Preprint. Discussion started: 6 September 2019

Biogeosciences Discussions
Open Access
EGU

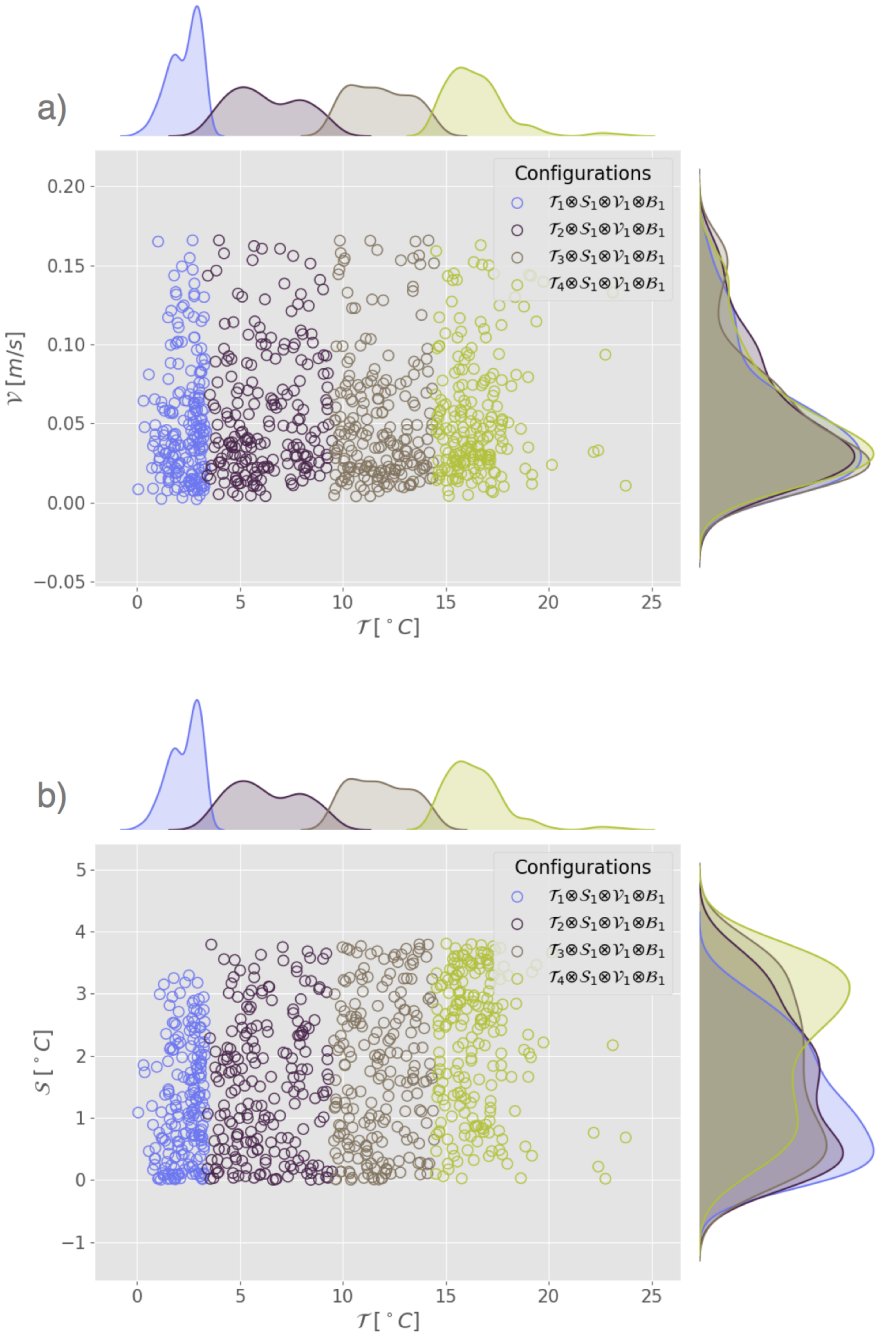

Figure 5. Scatter plot and marginal distribution from kernel density estimation in the plane (a) ($\mathcal{T}$,$\mathcal{V}$) and (b) ($\mathcal{T}$,$\mathcal{S}$) for the configurations corresponding to Exp. 3a, 3b, 3c and 3d from table 3.

https://doi.org/10.5194/bg-2019-353
Preprint. Discussion started: 6 September 2019

Biogeosciences Discussions Open Access EGU

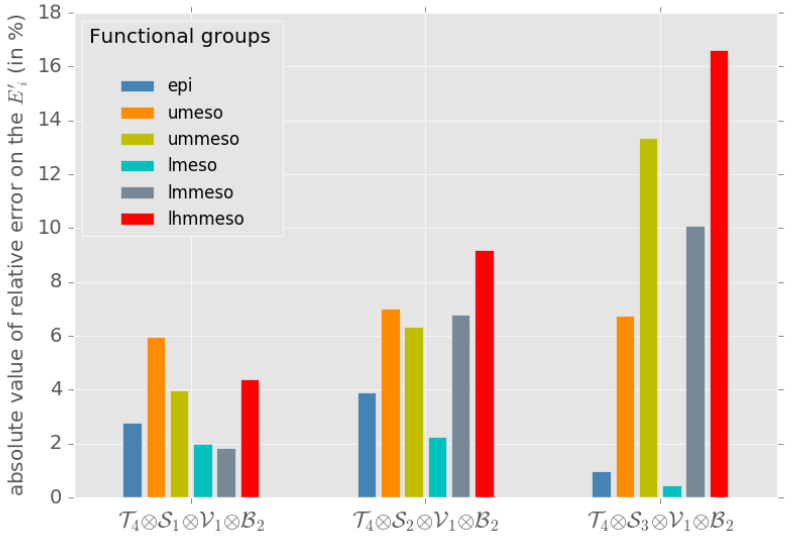

Figure 6. Mean relative error (E_r in %, Eq. 9) on each E'_i coefficients for Exp. 3a, 3b and 3c : comparison of weak, intermediate and high stratification in tropical temperatures, low velocity and no bloom regimes.

https://doi.org/10.5194/bg-2019-353
Preprint. Discussion started: 6 September 2019

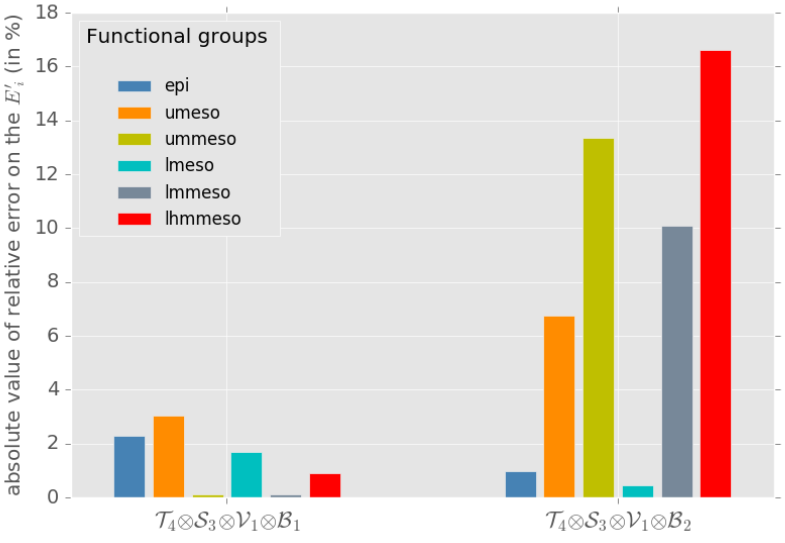

Figure 7. Mean relative error (E_r in %, Eq. 9) on each E'_i coefficients for Exp. 4c and 4d : bloom (4c) vs no bloom (4d) regimes in tropical temperatures, strong stratification and low velocities.

https://doi.org/10.5194/bg-2019-353
Preprint. Discussion started: 6 September 2019

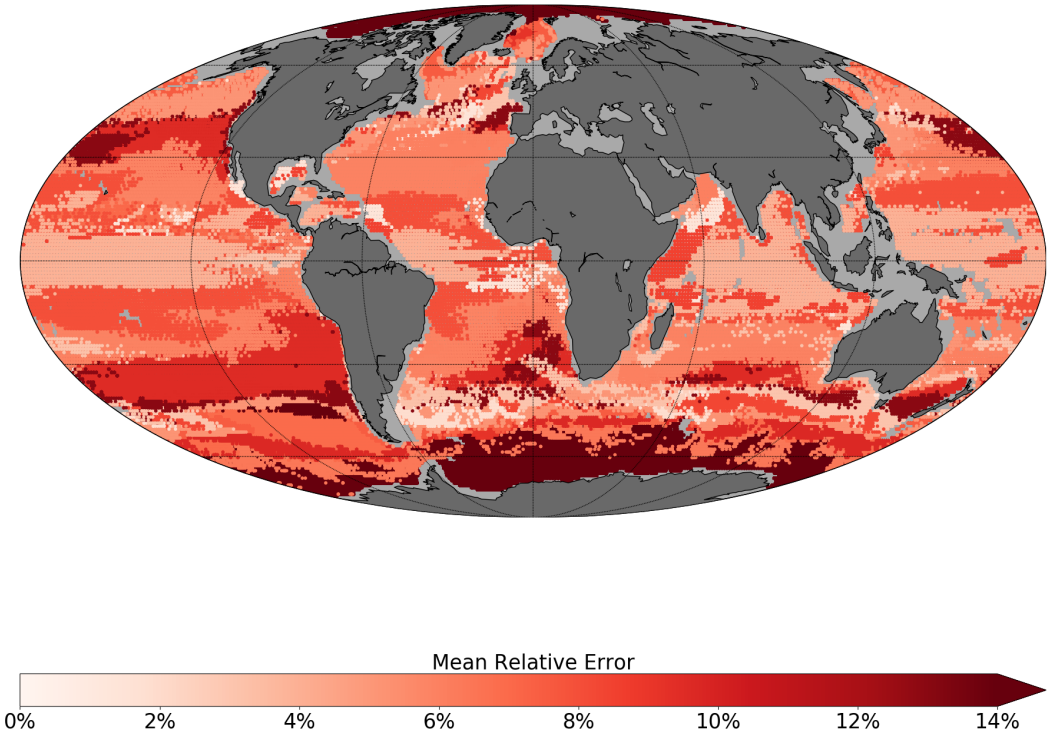

Figure 8. Averaged absolute value of relative error (E_r in %, Eq. 9) between the estimated and the target energy transfer parameters (E_i') according to the location of the chosen observation points in the twin experiment framework. Cells with no data have been shaded in grey.

https://doi.org/10.5194/bg-2019-353
Preprint. Discussion started: 6 September 2019

Biogeosciences
Discussions
Open Access
EGU

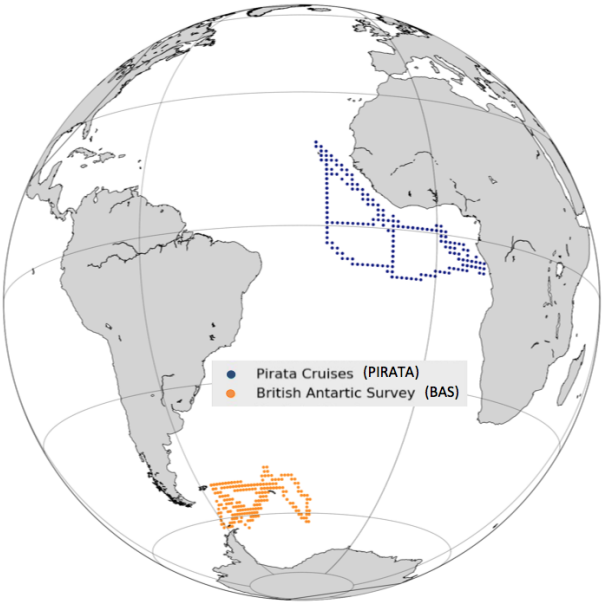

Figure 9. Map of PIRATA and BAS ship transects for the years 2013-2015.

https://doi.org/10.5194/bg-2019-353
Preprint. Discussion started: 6 September 2019

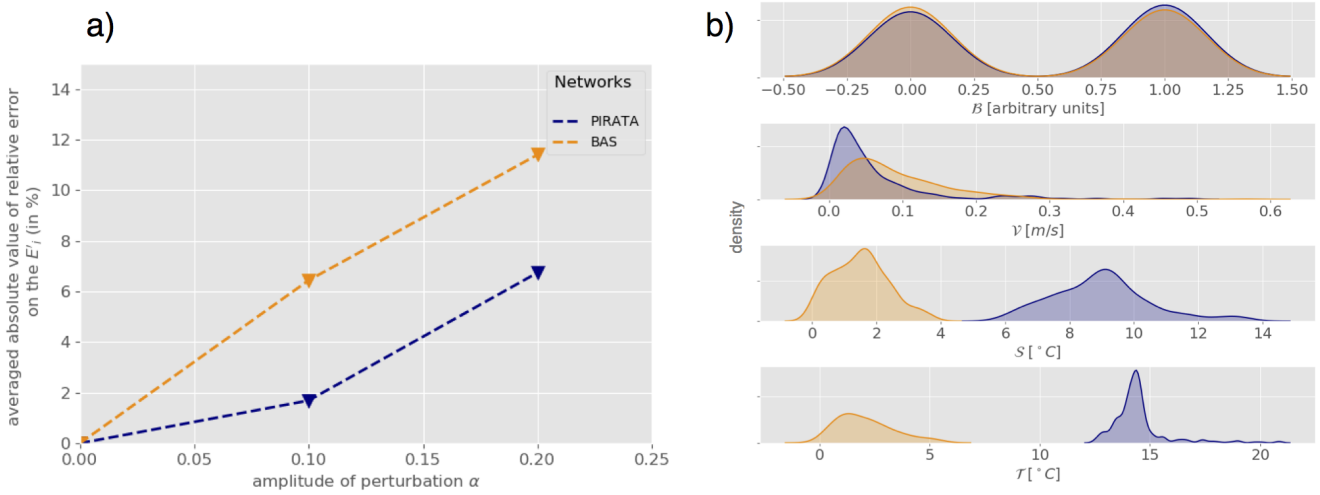

Figure 10. (a) Mean relative error on the coefficients E_r (in %, Eq. 9) as a function of the perturbation amplitude α (Eq. 8) for PIRATA (blue) and BAS (orange) observation networks. (b) Statistical distribution of all PIRATA (blue) and BAS (orange) observation location indicator variables : Bloom Index ($\mathcal{B}$), velocity norm ($\mathcal{V}$), stratification index ($\mathcal{S}$) and temperature ($\mathcal{T}$) estimated using kernel density estimation (Silverman, 2018).